Journal of Hazardous Materials 181 (2010) 170–180

Contents lists available at ScienceDirect

Journal of Hazardous Materials

journal homepage: www.elsevier.com/locate/jhazmat

Evaluation of five strategies to limit the impact of fouling in permeable reactive barriers

Lin Li [a,*], Craig H. Benson [b]

[a] Department of Civil and Environmental Engineering, Jackson State University, 1400 J.R. Lynch Street, P.O. Box 17068, Jackson, MS 39217, USA
[b] Department of Civil and Environmental Engineering, University of Wisconsin-Madison, WI 53706, USA

ARTICLE INFO

Article history:
Received 8 March 2009
Received in revised form 20 March 2010
Accepted 27 April 2010
Available online 4 May 2010

Keywords:
Permeable reactive barrier
Fouling
Reactive transport
Heterogeneity
Residence time

ABSTRACT

Ground water flow and geochemical reactive transport models were used to assess the effectiveness of five strategies used to limit fouling and to enhance the long-term hydraulic behavior of continuous-wall permeable reactive barriers (PRBs) employing granular zero valent iron (ZVI). The flow model accounted for geological heterogeneity and the reactive transport model included a geochemical algorithm for simulating iron corrosion and mineral precipitation reactions that have been observed in ZVI PRBs. The five strategies that were evaluated are pea gravel equalization zones, a sacrificial pre-treatment zone, pH adjustment, large ZVI particles, and mechanical treatment. Results of simulations show that installation of pea gravel equalization zones results in flow equalization and a more uniform distribution of residence times within the PRB. Residence times within the PRB are less affected by mineral precipitation when a pre-treatment zone is employed. pH adjustment limits the total amount of hydroxide ions in ground water to reduce porosity reduction and to retain larger residence times. Larger ZVI particles reduce porosity reduction as a result of the smaller iron surface area for iron corrosion, and retain longer residence time. Mechanical treatment redistributes the porosity uniformly throughout the PRB over time, which is effective in maintaining residence time.

1. Introduction

The permeable reactive barrier (PRB) is an in situ remediation technology where contaminated ground water is treated passively as it flows through a reactive medium. Most PRBs use granular zero valent iron (ZVI) to create redox conditions that result in degradation or immobilization of chlorinated solvents and herbicides, heavy metals, and radionuclides [1,2]. These redox conditions also promote precipitation of secondary minerals from ions typically in ground water (and some contaminants as well), a process referred to as fouling [3–7].

Laboratory column tests and field studies of PRBs containing ZVI have shown that the pH rises quickly near the entrance face and then levels off in the range of 9–10 [6–8]. Li et al. [16] reviewed the types and quantities of secondary minerals formed in PRBs and found that the most common minerals are magnetite, hematite, goethite, lepidocrocite, calcite, aragonite, siderite, green rust, ferrous hydroxide, ferrous sulfide, and marcasite. Calcium carbonates and siderite typically are found near the entrance face of a PRB, whereas magnetite, ferrous hydroxide, green rust and iron oxyhydroxides form throughout a PRB [3,8–11].

Fouling can cause porosity reductions in PRBs and reductions in hydraulic conductivity [5]. Variability in flow velocities due to geological heterogeneity can exacerbate the effects of fouling. These reductions in reactivity, porosity, and hydraulic conductivity of the ZVI cause reorientation of flow paths, changes in flow rate, seepage velocity, and residence times, and deterioration of treatment efficiency [12–15].

Porosity reductions caused by precipitation of secondary minerals generally are estimated based on volumes of secondary minerals observed in cores or based on stoichiometric calculations using measured changes in aqueous concentrations. A review of porosity reductions for eight PRBs reported by Li et al. indicates that the porosity reduction ranges from 0.0007 to 0.03 per year and depends on in situ geochemistry and flow condition [16]. The porosity reduction typically is greatest near the entrance face and then diminishes with distance into the PRB. For example, Wilkin et al. report that the porosity of the iron medium in the PRB at the US Coast Guard Support Center (Elizabeth City, NC) decreased by 0.032 within 25 mm from the entrance face after 8 years operation. However, 80 mm into the iron medium, the porosity reduction diminished to less than 0.00002 [6].

Field data also suggest that the accumulation of secondary minerals exhibits spatial variability in response to variations in geochemistry and flow rate. Morrison collected 70 cores from a PRB at Monticello, Utah and conducted solid-phase analyses to deter-

* Corresponding author. Tel.: +1 601 979 1092; fax: +1 601 979 4045.
E-mail addresses: lin.li@jsums.edu (L. Li), chbenson@wisc.edu (C.H. Benson).

0304-3894/$ – see front matter © 2010 Elsevier B.V. All rights reserved.
doi:10.1016/j.jhazmat.2010.04.113

mine the spatial distribution of solid-phase Ca, U, and V. Contour maps of the solid-phase concentrations show that greater precipitation occurred in zones near the middle and edges of the PRB and that mineral precipitation penetrated deeper into the PRB in these regions. For example, 0.25 m from the entrance face, the solid-phase concentration of Ca varied between approximately 15 and 45 g/kg, solid-phase U varied between approximately 70 and 800 mg/kg, and solid-phase V varied between approximately 85 and 460 mg/kg, with the highest concentrations near the centerline of the PRB and edges and the lowest near the quarter points [17].

In many applications, PRBs employing ZVI are expected to last decades. Thus, considerable interest exists regarding strategies to limit fouling and its impact on long-term performance of PRBs [10]. Five proposed are evaluated in this paper: (i) pea gravel equalization zones up gradient and down gradient of the reactive zone to equalize flows [4,18], (ii) placement of a sacrificial pre-treatment zone upstream of the reactive medium [17,19], (iii) pH adjustment [3,19], (iv) use of larger ZVI particles [3], and (v) periodic mixing of the ZVI to break up and redistribute secondary minerals [10,20]. Table 1 summaries the five strategies proposed to address fouling in the long-term performance of PRBs and their related laboratory studies and field applications.

The intent of this study was to identify five strategies to limit the impact of fouling on hydraulic performance of PRBs. The emphasis is on PRBs containing granular zero valent iron (ZVI) as the reactive medium, although the principles that were used could be adapted for other media. Developing a comprehensive geochemical reactive transport model was not an objective of this study, nor was identifying the underlying geochemical reactions and mechanisms that may contribute to mineral fouling. These issues have been addressed in other field, laboratory, and modeling studies.

1.1. Pea gravel equalization zones

Spatial variability in aquifer hydraulic properties has been shown to affect the distribution of flows in PRBs and the rate and distribution at which minerals precipitate in pores [18]. In specific field groundwater chemistry and flow velocity condition, regions with high flow rates may not show significant pH increases and more mineral precipitation [7]. For simplified, this study assumes that regions with high flow rates tend to accumulate minerals more quickly and foul more rapidly than regions where flows are slower under same geochemistry condition [18]. These regions of more rapid mineral accumulation can be minimized or eliminated when flows in the PRB are equalized. One strategy to equalize flows is to install pea gravel zones along the up gradient and down gradient faces of the ZVI [18].

Pea gravel zones have been used in several field PRBs [4,21,22], but their effectiveness is largely undocumented. A modeling study shows that pea gravel zones improve connectivity of permeable aquifer facies and exacerbate preferential flow through the PRB, but reduce the effects of flow heterogeneity [23]. Although the gravel is very permeable, the flow rate and residence time in the gravel is controlled by PRB or surrounding aquifer [23]. Benner et al. [24] also show that pea gravel equalization zones result in smaller residence times and redistribute flow from their modeling study.

1.2. Sacrificial pre-treatment zone

Pre-treatment zones consisting of a mixture of nearly inert granular material (e.g., sand or gravel) and ZVI have been used as sacrificial regions where pH and redox conditions can change and secondary minerals can form before ground water enters the reactive zone of a PRB [25]. For example, a 0.6-m-thick pre-treatment zone containing 13% ZVI and 87% gravel was installed along the upstream face of the 1.2-m-thick 100% ZVI reaction zone in a PRB at Monticello, UT, USA [17]. Similarly, a 0.6-m-thick mixing zone with 10% ZVI and 90% coarse sand was placed upstream of the ZVI reactive zone in the PRB at Dover Air Force Base, DE, USA [19].

Data collected after 32 months of operation suggest that minerals have formed in the pre-treatment zone of the PRB at Monticello. Solid-phase Ca concentrations in the gravel-ZVI zone are double those in the reactive zone (100% ZVI), and solid-phase U and V have only been detected in the gravel-ZVI zone [17]. The pre-treatment zone in the PRB at Dover Air Force Base removed all of the dissolved oxygen (DO) and nitrate and most of sulfate after a 27-mo period. The removal of DO, nitrate, and sulfate in the pre-treatment zone is believed to limit mineral precipitation in the reactive zone [19].

1.3. pH adjustment

Because the formation of secondary minerals is favored when the pH is elevated, controlling pH has been suggested as a means to reduce fouling [3]. One technique is to add buffering materials to the reactive medium that will release protons and decrease the elevated pH caused by iron corrosion [3,19].

Mackenzie et al. [3] conducted laboratory column tests where pH adjustment was attempted by blending 85% ZVI with 15% FeS (by weight) throughout a laboratory iron column. Adding FeS decreased the effluent solution pH by 1.0 after 165 pore volumes. Profiles of calcium and carbonate concentrations in the columns with and without FeS were similar over time, although the calcium and carbonate concentrations were expected to be approximately one order of magnitude higher in the column with the lower pH based on equilibrium calculations. Porosity reductions estimated from inorganic concentrations profiles and molar volumes were similar in the columns with and without FeS. The pH at the iron surface was unaffected by the bulk pH, and dominated precipitation of minerals [3].

A mixture of 10% pyrite (FeS_2) and 90% sand was placed up gradient of the ZVI in the PRB at Dover Air Force Base for pH adjustment [19]. The pyrite-sand mixture quickly removed DO, nitrate, and sulfate. The influent pH decreased by 1.0, but there was no effect on the pH in the reactive (100% ZVI) zone. The pH increased to 10.7 in the 100% ZVI reactive zone, which is the same pH attained in regions of the PRB without pH adjustment [19].

1.4. Large ZVI particles

Larger ZVI particles have smaller specific surface area (e.g., surface area per volume), which should result in less corrosion [3]. Mackenzie et al. [3] report that iron columns permeated with aerated ground water were quickly clogged by iron oxides. Mixing larger ZVI particles (1.0–4.6 mm) with smaller ZVI particles (0.4–1.0 mm) was attempted to minimize plugging in the front of ZVI columns. Pressure buildup measured in the column containing the mixing ZVI particles was only 25% of that at the column only containing with small ZVI particles after 50 h of operation [3].

1.5. Mechanical treatment

Mechanical methods such as auger mixing and ultrasonic treatment have been proposed to break up and dislodge mineral precipitates [10]. Geiger et al. treated the PRB at Cape Canaveral Air Station, FL, USA using two ultrasonic transducers inserted into the ZVI at depths of 0.18–0.66 m [20]. With 30 min duration of 40 kHz ultrasound or 90 min duration of 25 kHz ultrasound, mineral precipitates and corrosion products on the iron particles were partially removed. TCE degradation rates of recovered iron particles, determined in the laboratory, increased by 21–67% compared to iron particles before ultrasound treatment [20].

Table 1
Strategies of limiting fouling from PRBs studies.

Strategy	Description	Laboratory studies, field applications, references
Pea gravel equalization zones	Adding pea gravel zones up gradient and down gradient of the PRB	Moffett Federal Airfield, Mountain View, CA [18], Y-12 Site, Oak Ridge, TN [4].
Sacrificial pretreatment zone	Mixture of sand or gravel and ZVI placed in up gradient of the PRB	Former mill site, Monticello, UT [17], Dover Air Force Base, DE [19].
pH adjustment	Adjust pH in the PRB with pH buffering materials (e.g., ferrous sulfide, pyrite)	Ferrous sulfide to adjust pH in laboratory column [3], Pyrite (FeS_2) mixing with ZVI at Dover Air Force Base, DE [19].
Particle size adjustment	ZVI with larger particle size upstream of PRB	Laboratory column study [3]
Mechanical treatment	Mechanical break down of minerals in the ZVI	Cape Canaveral Air Station, FL [20].

Although some of these strategies have been attempted in laboratory studies and field installations, no systematic study has been conducted to date where the efficacy of these strategies is evaluated or compared. In this paper, the effectiveness of each strategy was evaluated in terms of its ability to limit fouling and the corresponding impact on hydraulic behavior of PRBs using a reactive transport model that simulates geochemical reactions and fouling in PRBs. The model was used to simulate flow and fouling in a PRB located in an aquifer with a natural level of heterogeneity so as to represent conditions that may occur during the service life of a typical PRB.

2. Ground water flow and reactive transport modeling

Equilibrium and kinetic models have been used to simulate geochemical processes and mineral formation in PRBs [26–29]. Equilibrium models are used to estimate the aqueous species and solid phases that exist in a state of thermodynamic equilibrium, but do not account for the rate at which the reactions occur and generally do not involve the movement of ground water. Kinetic models describe the rate at which geochemical reactions occur and output the aqueous and solid phase concentrations as a function of time. However, the geochemical reactions need to be specified by the user along with the reaction rate expressions and the rate coefficients. Kinetic models are appropriate when flow rates are not negligible relative to reaction rates. Reactive transport codes incorporating kinetic geochemical algorithms have been used by Mayer et al. [29], Li et al. [28], and Jeen et al. [27] for simulating contaminant degradation and mineral precipitation in PRBs. Kinetic model of Li et al. [28] was selected in this study to simulate geochemical processes and mineral formation in PRBs.

The conceptual model is a horizontal PRB and a portion of the surrounding aquifer (Fig. 1). The hydraulic conductivity of the aquifer is spatially variable to represent the heterogeneity inherent in natural systems. The PRB is oriented perpendicular to the primary direction of ground water flow and is composed of ZVI particles.

As ground water flows through the PRB, the iron is corroded by dissolved oxygen (DO), water, nitrate, and sulfate, which elevates the pH and causes secondary mineral precipitation. Iron corrosion is assumed to produce ferrous iron (ferric iron is not included), because ferrous iron is more commonly observed in field studies [30–32]. Ground water is assumed to be in chemical equilibrium (i.e., no reactions occurring) before entering the PRB. No solid phases are carried into the PRB from inflowing ground water. Ground water flowing into the PRB is assumed to be in chemical equilibrium and includes Fe^{2+}, Ca^{2+}, Mg^{2+}, NO_3^-, SO_4^{2-}, H^+, OH^-, HCO_3^-, CO_3^{2-}, and dissolved O_2. These dissolved species are assumed to form six minerals in the PRB: aragonite or calcite ($CaCO_3$), magnesite ($MgCO_3$), siderite ($FeCO_3$), ferrous hydroxide ($Fe(OH)_2$ (am)), ferrous sulfide (FeS (am)), and brucite ($Mg(OH)_2$). Ferrous hydroxide eventually may convert to magnetite (Fe_3O_4) [33], but the transformation conditions are still in debate [34,35]. Consequently, the conversion was not included in the model.

Using only six minerals in the model is a simplification of the actual geochemical environment, but is consistent with the formulations used by Mayer et al. [29]. Developing a model that accurately simulates all geochemical processes was not within the scope of this study. Rather, the intent was to evaluate the strategies to limit the impact of fouling in PRBs on their long-term hydraulic behavior. Nevertheless, the six minerals are the most common minerals found in column and field studies of PRBs (see review by Li et al. [16]). Thus, the use of only six minerals is unlikely to impact predictions regarding the general degree of mineral fouling occurring in PRBs, and how fouling affects hydraulic behavior.

When ground water containing high DO, the influent ground water can rapidly reacts with zero valent iron and drives the formation of various ferric oxide, oxyhydroxide, and hydroxide mineral. The rapid cementation and loss of pore space and hydraulic conductivity occurs due to precipitation of ferric-ion bearing minerals. However, most field PRBs are anoxic/anaerobic condition with low DO and thus oxidative iron corrosion reactions are inadequate [5,7]. The oxidation process in this modeling study is excluded.

The model only considers mineral fouling. The effects of hydrogen or nitrogen gas evolution, which can result in blockage of pores to water flow, are not incorporated. Some studies have suggested that gas evolution can have an appreciable effect on the hydraulic behavior of PRBs (e.g., Mackenzie et al. [3]; Kamolpornwijit et al. [12]). Thus, gas evolution may exacerbate the effects predicted by the model described herein.

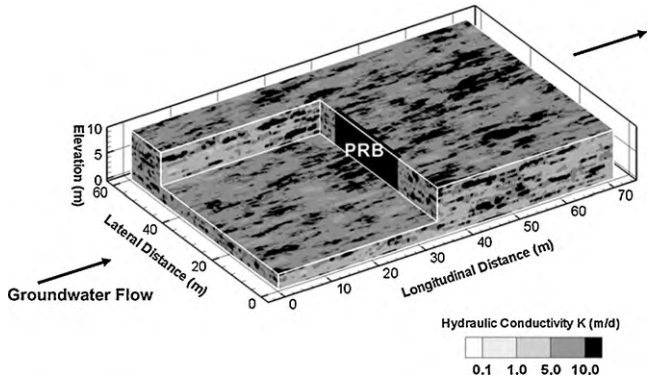

Fig. 1. Heterogeneous aquifer containing PRB that was simulated in study (K_g = 3.9 m/d, $\sigma_{\ln K}$ = 1.0, λ_l = 3.0 m, λ_t = 1.0 m, λ_v = 0.5 m, and K_p = 216 m/d).

The model incorporates selected acid/base and redox reactions, but ignores aqueous metal complexes and contaminant transformation reactions. Metal complexes were not included because a series of equilibrium analyses conducted with MINTEAQ2 [36] over a range of pH and temperatures expected in PRBs showed that more than 90% of Ca and Mg existed as free metal ions. Although Fe-complexes may dominate in some situations, to simplify the model, Fe(II) was assumed to exist only as free ions (Fe^{2+}). This assumption may overestimate the availability of Fe^{2+} ions and thus over-predict mineral precipitation, which is a conservative approach when assessing mineral fouling of PRBs. In cases where, metal complexes cannot be ignored, a more comprehensive geochemical model (e.g., MIN3P, Mayer et al. [29]) should be used. Contaminant transformations were ignored because the amount of iron corrosion and mineral precipitation caused by reduction of chlorinated compounds or toxic heavy metals generally is negligible relative to that due to other processes, even though the transformations are intrinsic to the remediation process [6,17].

Flow and transport in the PRB and the surrounding region of the aquifer were simulated using the ground water flow model MODFLOW [37] and the reactive transport model RT3D [38]. A geochemical algorithm developed by Li et al. were added to RT3D for simulating the reaction kinetics associated with the redox and mineral precipitation–dissolution reactions that occur in PRBs [28]. Li et al. describe in detail how the combination of MODFLOW and RT3D is used to simulate flow, transport, and geochemical reactions in PRBs and show that predictions made with the MODFLOW-RT3D model are in general agreement with field data from PRBs [28]. A summary is presented in this section of the key aspects of the model.

A three-dimensional domain was used to simulate flow in the PRB and the surrounding aquifer. Heterogeneity in the aquifer hydraulic conductivity was simulated using the turning bands random field generator described in Elder et al. [23]. The intent was to generate a reasonably realistic three-dimensional distribution of aquifer hydraulic conductivity (i.e., single realization) simulating the heterogeneity inherent in natural aquifers. The generator was not used to create multiple stochastic realizations for a probabilistic analysis. Hydraulic conductivity of the aquifer was assumed to be log-normally distributed and was characterized by the geometric mean hydraulic conductivity (K_g), the standard deviation of the logarithm of hydraulic conductivity ($\sigma_{\ln K}$), and the correlation lengths along the longitudinal (λ_l), transverse (λ_t), and vertical (λ_v) axes [23]. For the simulation described in this paper, $K_g = 3.9$ m/d, $\sigma_{\ln K} = 1.0$, $\lambda_l = 3$ m, $\lambda_t = 1$ m, and $\lambda_v = 0.5$ m. The vertical variability in the properties of hydraulic conductivity at the upgradient or downgradient aquifer was represented by the correlation length along vertical axes of 0.5 m. The system with vertical variability can simulate the zones of high conductivity that can overwhelm the iron media and lead to rapid breakthrough.

A continuous-wall PRB is located in the middle of the domain (Fig. 1). The PRB is oriented perpendicular to the average direction of ground water flow and is 10 m deep, 25 m wide, and 1 m thick. The PRB is assumed to have uniform hydraulic conductivity (K_p) at the time of installation (216 m/d for the base case). The initial porosity of the ZVI was set at 0.60, which falls within the typical range for porosity of ZVI (0.55–0.65) reported for the porosity of ZVI [10,15]. The porosity of ZVI is large relative to granular media having similar particle size because of the angularity and oblong shape of ZVI particles. Total and effective porosities of the ZVI were assumed to be equal based on tracer tests reported by Kamolpornwijit et al. [12] and Vikesland et al. [13].

2.1. Ground water flow modeling

Steady-state flow was simulated in the heterogeneous aquifer and PRB using MODFLOW. The model domain consisted of 250 columns, 120 rows, and 20 layers, which represents a flow domain of 71 m × 60 m × 10 m. The grid spacing was 0.5 m in the vertical and lateral directions. In the longitudinal (flow) direction, the grid size varied from 0.3 to 0.1 m, with the smaller spacing (0.1 m) being used within the PRB. The size of the domain and the level of discretization were determined based on a parametric analysis, which is described in Li et al. [28]. This analysis identified the domain size needed so that flow and transport in the vicinity of the PRB were not affected by the boundaries and the grid spacing needed to accurately represent the flow paths and residence times in the PRB. Unconfined flow was assumed with specified-head boundaries set along the east and west ends of the aquifer (Fig. 1). An average hydraulic gradient of 0.01 was imposed to yield seepage velocities ranging from 0.05 to 0.40 m/d, which are typical conditions observed in the field during PRB studies [7]. No-flow boundaries were used for the lateral, top, and bottom boundaries.

The flow field is updated annually to account for changes in hydraulic conductivity of the PRB caused by mineral precipitation using a Kozeny–Carman formulation to relate changes in porosity to changes in hydraulic conductivity [27,39]. A sensitivity analysis conducted by Li et al. [28] showed that errors in the porosity reduction were limited to less than 1% when the hydraulic conductivity was updated annually.

2.2. Reactive transport modeling

Reactive transport was simulated with RT3D, which uses the head solution from MODFLOW as input. The transport modeling domain was a subdomain of that used for flow modeling and consisted of the PRB and a small region of the surrounding aquifer. A parametric analysis was conducted to determine the minimum size of the transport domain where the boundaries would not influence transport within the PRB. Based on this analysis, the upstream boundary was located 0.1 m up gradient of the entrance face, the downstream boundary was located 0.2 m down gradient from the exit face, and the side boundaries were located 0.5 m from the sides of the PRB.

The transport time step was automatically adjusted by RT3D to ensure that the cell-based Courant number was less than 1.0 [40]. Heterogeneity in the hydraulic conductivity of the aquifer was assumed to be the source of macroscopic dispersion [41]. Microscopic dispersion caused by pore-scale mixing was simulated using a small dispersivity (0.0007 m). The molecular diffusion coefficient was assumed to be 3×10^{-5} m^2/d [42].

The initial concentration of each species in the PRB was assumed to be zero. The upstream boundary was assigned the concentration of ions in ground water and was assumed to be spatially uniform and time invariant. The bottom boundary was assigned as no flux. All other boundaries were assigned a Cauchy boundary condition with no dispersive flux [40].

2.3. Geochemical algorithm

The geochemical algorithm is described in detail by Li et al. [28]. A synopsis is provided here. A summary of the geochemical reactions and their reaction rates is summarized in Table 2. There are three redox reactions related to iron corrosion, an equilibrium reaction between bicarbonate and carbonate ions, dissociation of water, six mineral precipitation–dissolution reactions, and one reaction for microbial sulfate reduction. All of the geochemical reactions are assumed to occur in parallel and are solved simultaneously. The concentration of each species is calculated for each cell in the

Table 2
Reactions included in geochemical algorithm with kinetic rate expressions, and solubility constants.

Reactions	Mineral formed	Kinetic rate expression[a]	Solubility constant log(K_{eq})[b]
Iron corrosion			
$Fe^0 + 2H_2O \rightarrow Fe^{2+} + H_2\,(aq) + 2OH^-$	–	$k_{an,Fe}S$	–
$4Fe^0 + 7H_2O + NO_3^- \rightarrow 4Fe^{2+} + 10OH^- + NH_4^+$	–	$k_{NO}Sa_{NO_3^-}$	–
$SO_4^{2-} + 4H_2\,(aq) \rightarrow HS^- + OH^- + 3H_2O$[c]	–	$-k\left(\frac{[SO_4^{2-}]}{K_{SO_4}+[SO_4^{2-}]}\right)\left(\frac{[H_2(aq)]}{K_{H_2}+[H_2(aq)]}\right)$	–
Secondary mineral precipitation–dissolution			
$CaCO_3\,(s) \leftrightarrow Ca^{2+} + CO_3^{2-}$	Aragonite/calcite	$-k_{Ca}(1 - a_{Ca^{2+}}a_{CO_3^{2-}}/K_{eq})$	−8.1
$MgCO_3\,(s) \leftrightarrow Mg^{2+} + CO_3^{2-}$	Magnesite	$-k_{Mg}(1 - a_{Mg^{2+}}a_{CO_3^{2-}}/K_{eq})$	−7.2
$Mg(OH)_2\,(s) \leftrightarrow Mg^{2+} + 2OH^-$	Brucite	$-k_{Mg2}(1 - a_{Mg^{2+}}a^2_{OH^-}/K_{eq})$	−11.2
$FeCO_3\,(s) \leftrightarrow Fe^{2+} + CO_3^{2-}$	Siderite	$-k_{Fe1}(1 - a_{Fe^{2+}}a_{CO_3^{2-}}/K_{eq})$	−10.5
$Fe(OH)_2\,(am) \leftrightarrow Fe^{2+} + 2OH^-$	Ferrous hydroxide	$-k_{Fe}(1 - a_{Fe^{2+}}a^2_{OH^-}/K_{eq})$	−15.2
$FeS\,(am) + H_2O \leftrightarrow Fe^{2+} + HS^- + OH^-$	Ferrous sulfide	$-k_{FeS}(1 - a_{Fe^{2+}}a_{HS^-}a_{OH^-}/K_{eq})$	−18.4

[a] k is rate coefficient, S is reactive surface area of ZVI, a is activity of aqueous species, and K_{eq} is solubility constant. Activity coefficients were calculated using the extended Debye–Hückel equation.
[b] Calculated based on data from Krauskopf and Bird [52] and Stumm and Morgan (1996) [43] at 15 °C and 101 kPa. aer = aerobic, an = anaerobic.
[c] Half-saturation constants for SO_4^{2-} and H_2 (aq).

domain during each time step. Activity corrections were made with the extended Debye-Hückel equation [43].

A pseudo-first order reaction rate proportional to the reactive surface area of ZVI and the nitrate concentration was assumed for iron corrosion [29,32]. For iron corrosion by water, the reaction rate was assumed to be proportional only to the reactive surface area of ZVI [35,53]. The rate of degradation of sulfate to HS^- by sulfate-reducing bacteria (e.g., as observed in PRBs in [6]) was assumed to follow the Monod equation, as was done by Mayer et al. [29]. Kinetics of mineral precipitation–dissolution was assumed to follow transition state theory [44,45]. Comparisons between field data and model predictions by Mayer et al. [29], Mayer et al. [46], and Li et al. [28] indicate that this approach reasonably replicates conditions in PRBs. The mineral reactions and their solubility constants are summarized in Table 2.

Minerals precipitates formed in the iron medium were assumed to be immobile and the pore space occupied by the minerals was estimated from the molar volume of each mineral. The pore volume reduction at a given location was computed as the total pore volume occupied by the mineral precipitates at the location less the pore volume gained by dissolution of iron. The porosity reduction was calculated as the pore volume reduction in a finite-difference grid cell divided by the cell volume.

The reactive surface area of the ZVI was reduced over time to account for dissolution of iron and deposition of minerals on the surface of the ZVI. The effect of iron dissolution was simulated using the method employed by Mayer et al. [29]. Reduction of reactive surface area due to mineral precipitation was computed using the method described in Morrison [17] and Mayer et al. [29]. Reductions in the hydraulic conductivity of the ZVI were estimated using the Kozeny–Carmen equation:

$$K_{pt} = K_{po}\frac{[n_o - \Delta n_t/n_o]^3}{[1 - n_o + \Delta n_t/1 - n_o]^2} \quad (1)$$

where n_o is initial porosity, K_{po} is initial hydraulic conductivity, and n_t is the reduction in porosity at time t. The reduction in hydraulic conductivity predicted by Eq. (1) is non-linearly related to the porosity reduction (i.e., the rate of decrease in hydraulic conductivity increases as the porosity reduction becomes larger). Only mineral precipitates were assumed to contribute to the change in porosity. The effects of gas evolution and accumulation and biological matter were ignored due to difficulties in modeling these effects. Gas and biological matter may exacerbate the effects of the porosity reductions reported herein, although field data to date do not indicate that either has an appreciable effect on PRBs. Other hydraulic conductivity models could have been used to develop an expression like Eq. (1) [17,47,48]. However, none of the models has been shown to be superior for predicting changes in the hydraulic conductivity of ZVI. A review of how hydraulic properties can change in response to fouling is in Saripalli et al. [49].

2.4. Residence time

Residence times within the PRB were defined using the particle tracking code Path3D [50], which uses the head solution from MODFLOW as input. One thousand particles were released from a source of 25 m wide by 10 m deep that was located 20 m up gradient from the PRB. Path3D calculates the position and travel time of each particle by moving particles through a series of time steps. The residence time of each particle in the PRB was calculated as the difference between travel times corresponding to entry and exit of the PRB.

3. Model validation

A comparison was made between model predictions and field data from one case study to verify that the user-defined reaction module in RT3D produces reasonable results. The PRBs at Moffett Federal Airfield was selected because the hydrological and geochemical conditions at this site are well defined [51]. Field observations were used to describe the aqueous species and mineral precipitates in each model. The kinetic reaction rate coefficients were initially estimated, but ultimately were calibration parameters because of the absence of information and potential variability of in situ rate coefficients. The calibrated rate coefficients were obtained by trial-and-error.

A pilot-scale funnel-and-gate PRB consisting of granular iron was installed in 1996 at Moffett Federal Airfield to remove TCE and DCE from ground water [51]. The gate is 3.0-m long (orthogonal to flow direction), 3.0-m wide (along the flow direction), and 5.5-m deep. The gate consists of a 1.8-m thick barrier of granular ZVI sandwiched between two 0.6-m-thick layers of pea gravel (up gradient and down gradient sides).

Ground water samples were collected between April 1996 (installation) and October 1997 and analyzed for target contaminants, pH, major cations and anions, and indicator parameters [51]. Analysis of core samples showed that magnetite (Fe_3O_4), hematite (α-Fe_2O_3), aragonite ($CaCO_3$), and marcasite (FeS_2) formed in the iron media. No direct measurements were made of siderite ($FeCO_3$), FeS, $Fe(OH)_2$ (am), $Fe(OH)_3$, brucite ($Mg(OH)_2$), or green rust, but Yabusaki et al. estimated amounts of these secondary minerals based on stoichiometry using changes in aqueous concentrations in the PRB [51].

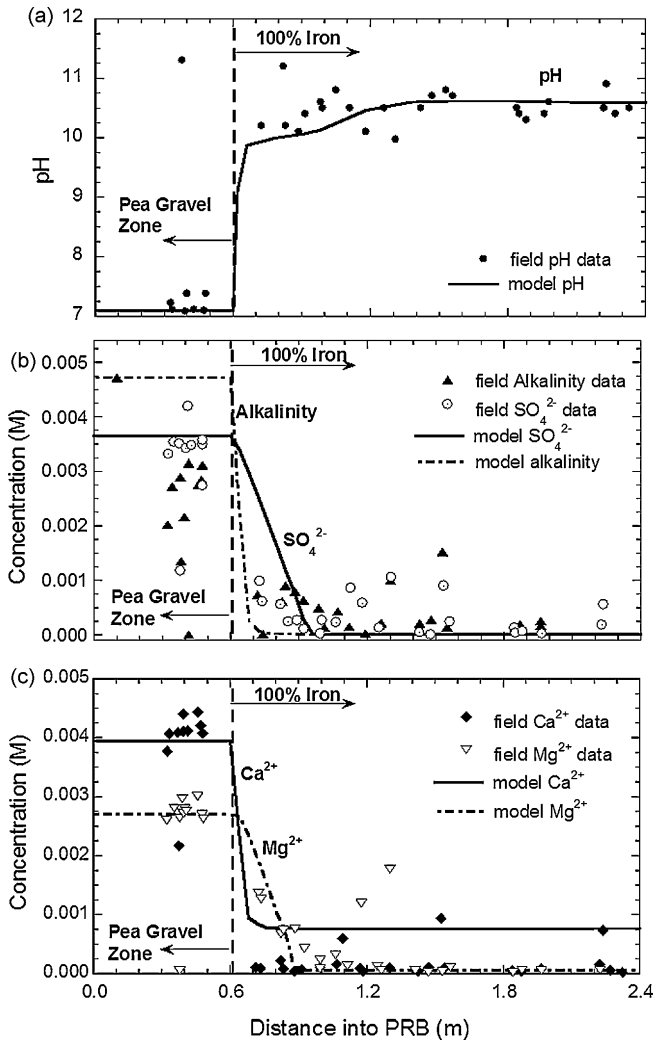

Fig. 2. Measured data and predicted concentrations for the pilot-scale PRB installed at Moffett Federal Airfield, Mountain View, CA, USA after 1 year of operation: (a) pH, (b) alkalinity and SO_4^{2-}, and (c) Ca^{2+} and Mg^{2+}.

The MODFLOW-RT3D model was adapted to simulate the nearly one-dimensional conditions in the gate at the Moffett Federal Airfield site using input data provided in Yabusaki et al. [51]. MODFLOW was used to simulate steady-state flow in the pea gravel zones and iron media zone. The initial hydraulic conductivity in the PRB was 186 m/d and the porosity was 0.66. The hydraulic conductivity in the pea gravel zones was 86.4 m/d. A hydraulic gradient of 0.0003 was applied across the PRB to yield the Darcy velocity 0.04 m/d reported in Yabusaki et al. [51].

Five minerals reported by Yabusaki et al. were included in the model: $CaCO_3$, $FeCO_3$, $Fe(OH)_2$ (am), $Mg(OH)_2$, and FeS (am) [51]. Since the DO at Moffett Federal Airfield is less than 0.1 mg/L, $Fe(OH)_3$ and green rust were not included. The composition of ground water entering the PRB, shown in Table 3, was based on information provided in Yabusaki et al. [51]. The effective rate coefficients were adjusted to reproduce the measured solution pH, alkalinity, and concentrations of sulfate, calcium, and magnesium after 1 year of operation [28]. The calibrated reaction rate coefficients are summarized in Table 4 along with ranges based on data reported in the literature. In general, the calibrated rate coefficients fall within the ranges from the literature (Table 4).

Comparisons of the predicted and measured pH and concentration profiles are shown in Fig. 2. The predicted pH is in general agreement with the observed pH (Fig. 2a), including the rapid increase in pH as ground water enters the ZVI and the leveling out in the interior. The drop in alkalinity (defined as $[HCO_3^-]+2[CO_3^{2-}]+[OH^-]-[H^+]$) just up gradient of the PRB is not captured (Fig. 2b), but the alkalinity predicted by RT3D inside the PRB is similar to that measured in the field. The sulfate concentration predicted by RT3D also is in general agreement with the trends observed in the field (Fig. 2b), as are the Ca^{2+} and Mg^{2+} concentrations. However, the predicted Ca^{2+} concentrations in the PRB are near the upper bound of the measured concentrations (Fig. 2c).

4. Effectiveness of five strategies

A series of simulations were conducted to evaluate the five strategies for limiting fouling and its impact on hydraulic behavior of PRBs. The model was the same as that used to simulate the gate at Moffett Federal Airfield. Ion concentrations in the inflowing ground water are summarized in the column labeled "base case" in Table 3 and the rate coefficients are summarized in a similar column in Table 4. Impact of these strategies on hydraulic properties and behavior of PRBs is evaluated in terms of porosity reductions in the ZVI and residence times. Simulations were conducted for 30 years of operation, which is a common upper bound of anticipated service life for PRBs [5,10].

In the evaluation of five strategies, the mass flux out of PRB and installation cost issues were not addressed.

4.1. Pea gravel equalization zones

Simulations were conducted to assess the effectiveness of pea gravel equalization zones by adding 0.5-m-thick zones having a hydraulic conductivity of 864 m/d and porosity of 0.4 directly up gradient and down gradient of the 1-m-thick PRB with 100% ZVI. The pea gravel zones had the same lateral and vertical dimensions as the PRB (25-m wide and 10-m deep). Thickness and hydraulic conductivity of gravel zones were selected to be consistent with the gravel zones used for the PRB at Moffett Federal Airfield [18].

Average and maximum porosity reductions in the PRB (100% ZVI reactive zone) with and without the pea gravel zones are shown in Fig. 2 as a function of distance from the entrance face of the PRB after 30 years. The average porosity reduction in Fig. 2 is the arithmetic mean of the porosity reduction in all cells comprising the PRB at a given distance from the entrance face. The maximum porosity reduction is the largest porosity reduction in all cells at a particular distance from the entrance face. The observed trends are a function of the selected groundwater composition and the selected hydrogeologic model. It is the trends that are most important, and not the absolute numbers determined from the model.

The average porosity reduction reaches a peak near the entrance face, which is followed by a decrease and then leveling off (≈0.7 m from the entrance face) (Fig. 2). The maximum porosity reduction persists farther into the PRB, and diminishes less rapidly than the average porosity reduction, because mineral forming ions are being transported deeper into the PRB along preferential flow paths due to flow heterogeneity. The shape of these porosity reduction profiles reflects the precipitation of carbonate minerals near the entrance face of the PRB and ferrous hydroxide in the midsection and rear of the PRB [28]. Carbonate minerals precipitate in the upstream half of the PRB, with peak porosity reduction by these minerals at the entrance face. Precipitation of the carbonate minerals drops to insignificant levels near the mid-plane due to carbonate depletion [28]. In contrast, $Fe(OH)_2$ (am) precipitates throughout the PRB due to the availability of the corrosion products Fe^{2+} and OH^-, both of which are formed throughout the PRB due to iron corrosion [28].

Table 3
Concentrations of aqueous species in influent ground water.

Aqueous species in influent ground water	Aqueous species concentrations at Moffett Federal Airfield (M)	Aqueous species concentrations at base case (M)
Fe^{2+}	9.0×10^{-7}	9.0×10^{-7}
Ca^{2+}	3.9×10^{-3}	1.0×10^{-3}
Mg^{2+}	2.7×10^{-3}	1.0×10^{-3}
OH^-	1.3×10^{-7}	1.0×10^{-7}
Alkalinity (HCO_3^-)	4.7×10^{-3}	1.0×10^{-3}
NO_3^-	3.9×10^{-5}	1.0×10^{-5}
Cl^-	8.4×10^{-3}	9.9×10^{-4}
SO_4^{2-}	3.6×10^{-3}	1.0×10^{-3}

Table 4
Rate coefficients used in simulations.

Reactions terms	Units	Moffett Federal Airfield[a]	Base case	Rate coefficients reported in literature	Sources[b]
Water[c]	$mol/m^2/d$	7.0×10^{-7}	2.0×10^{-7}	3.0×10^{-8} to 5.4×10^{-3}	[1–3,5,9]
Nitrate[c]	$m^3/m^2/d$	2.6×10^{-5}	1.0×10^{-4}	1.8×10^{-8} to 2.8×10^{-5}	[1,4,6–8]
Microbial sulfate reduction[d]	m/d	1.0×10^{-3}	1.0×10^{-5}	5.0×10^{-6} to 5.0×10^{-3}	[1,4–6,10]
$CaCO_3$	m/d	1.0×10^{-4}	1.0×10^{-4}	2.7×10^{-9} to 1.4×10^{-4}	[1,2,7,11]
$FeCO_3$	m/d	1.1×10^{-5}	1.0×10^{-4}	1.1×10^{-5} to 2.7×10^{-4}	[1,2,11]
$Fe(OH)_2$ (am)	m/d	5.1×10^{-5}	1.0×10^{-4}	$<2.2 \times 10^{-4}$	[1,2]
FeS (am)	m/d	1.0×10^{-6}	1.0×10^{-6}	1.1×10^{-8} to 2.2×10^{-5}	[1,2,11]
$MgCO_3$	m/d	NA	1.0×10^{-4}	1.1×10^{-8} to 1.4×10^{-4}	[1,11]
$Mg(OH)_2$	m/d	2.0×10^{-3}	1.0×10^{-5}	3.4×10^{-6}	[2]

NA: no available.
[a] After calibration with field measurements.
[b] 1. Mayer et al. (2001); 2. Yabusaki et al. (2001); 3. Reardon (1995); 4. Gu et al. (2002); 5. Gu et al. (1999); 6. Gandhi et al. (2002); 7. Alowitz and Scherer (2002); 8. Westerhoff (2003); 9. Chen et al. (2001); 10. Kober et al. (2002); 11. Hunter et al. (1998).
[c] Reactive surface area of ZVI set at 3.9×10^6 m^2/m^3.
[d] Half-saturation constants for SO_4^{2-} and H_2 (aq) were $K_{SO_4} = 10 \times 10^{-4}$ M, and $K_{H_2} = 10 \times 10^{-7}$ M, respectively.

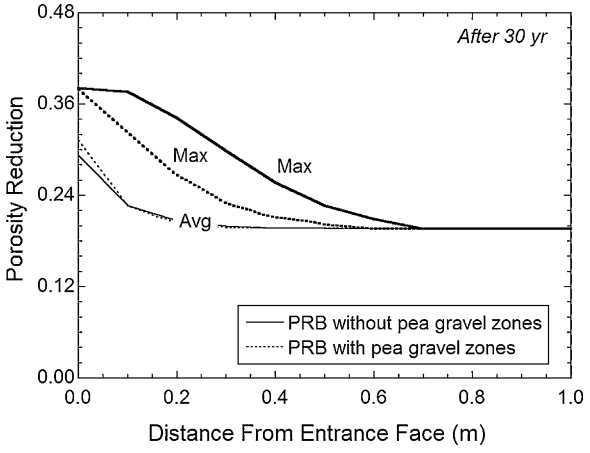

Fig. 3. Maximum and average porosity reduction as a function of distance from the entrance face of the PRB with and without pea gravel zones.

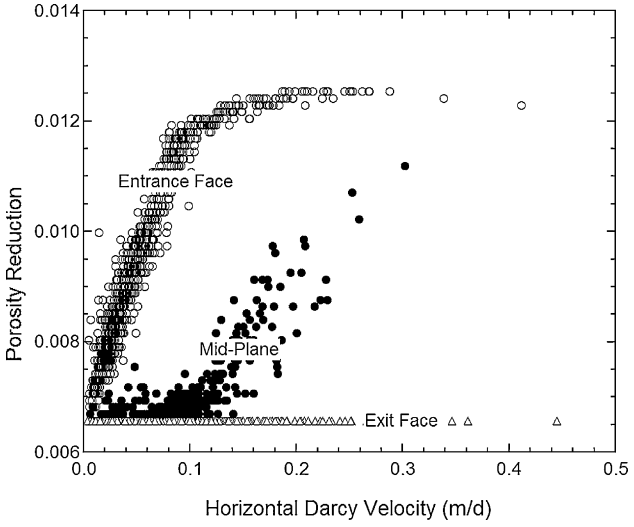

Fig. 4. Porosity reduction at entrance face, mid-plane, and exit face of PRB after 1 year of operation as a function of Darcy velocity (base case parameters).

The differences between the maximum and average porosity reductions shown in Fig. 3 are caused by variations in ground water velocity. This effect is shown in Fig. 4 in terms of porosity reduction at the entrance and exit faces and the mid-plane of the PRB as a function of Darcy velocity. Each point in Fig. 4 corresponds to a single finite difference cell in the PRB. The sensitivity to Darcy velocity reflects the rate at which mineral forming ions are being delivered as well as the balance between mass delivery rates and geochemical reaction rates. Near the entrance face, larger porosity reductions occur at higher Darcy velocities. However, after the Darcy velocity reaches approximately 0.2 m/d, the porosity reduction drops slightly with increasing velocity. A similar pattern of porosity reduction exists at the mid-plane, but the porosity reduction increases with Darcy velocity only if the velocity is ≥0.1 m/d. In contrast, there is no relationship between porosity reduction and Darcy velocity at the exit face.

Pea gravel equalization zones result in a slight increase in average porosity reduction, and have no effect on the peak maximum porosity reduction (Fig. 3). However, from the entrance face, the maximum porosity reduction is lower with pea gravel zones. Flow equalization by the pea gravel zones reduces the prevalence and impact of preferential flow paths, which control maximum porosity reductions deeper in the reactive zone of PRBs [16].

Box plots showing the distribution of residence time in the PRB with and without pea gravel zones at the onset of operation and after 30 years are shown in Fig. 5. The centerline in the box corresponds to the median (50th percentile), the outer edges of the box correspond to the 25th and 75th percentiles, and the whiskers correspond to the 10th and 90th percentiles of the residence time.

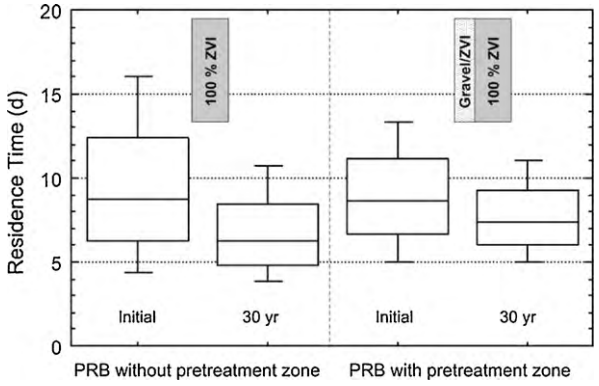

Fig. 5. Box plots of residence time in the PRB initially and after 30 years of operation with and without pea gravel zones.

Installation of pea gravel zones results in more uniform residence times (4.4–16.0 d compared vs. 5.9–12.7 d with pea gravel zones), but no change in the median residence time remains (8.8 d without pea gravel zones, 8.9 d with pea gravel zones). More importantly, addition of pea gravel zones reduces the frequency of very short residence times, which can have the greatest impact on fouling as well as quality of groundwater downstream of the PRB. This effect is realized initially and after 30 years, with more complete equalization as the PRB ages.

4.2. Sacrificial pre-treatment zone

Simulations to evaluate sacrificial pre-treatment zones were conducted with a 0.5-m-thick gravel-ZVI mixture placed directly up gradient of a 1-m-thick reactive zone containing 100% ZVI. The sacrificial pre-treatment zone had the same lateral and vertical dimensions as the 100% ZVI zone. The percentage of ZVI (13% by volume) and the porosity (0.4) of the pre-treatment zone at Monticello, UT [17] were used as input. Hydraulic conductivity of the pre-treatment zone was set at 640 m/d, which falls between typical hydraulic conductivities of gravel and ZVI.

Maximum porosity reductions in the reactive zone after 30 years with and without a sacrificial pre-treatment zone are shown in Fig. 6a as a function of distance from the entrance face. Including a pre-treatment zone reduces the maximum porosity reduction within the PRB by shifting precipitation into the pre-treatment zone. The effect of mineral precipitation on the pre-treatment zone is modest, with a maximum porosity reduction of only 0.06.

The shift in porosity reductions is caused by precipitation of carbonate minerals in the pre-treatment zone (Fig. 6b) due to elevated pH (Fig. 6c). HCO_3^- is consumed when minerals precipitate in the pre-treatment zone, thereby limiting the amount of HCO_3^- available for precipitation of carbonate minerals in the reactive zone (Figs. 6c). This effect could be enhanced by adding more ZVI to the pre-treatment zone. However, even if the ZVI content was increased, precipitation within the reactive zone would not be eliminated, as $Fe(OH)_2$ will form in response to corrosion of iron within the reactive zone (Fig. 6b).

Box plots of residence times in the PRB with and without the sacrificial pre-treatment zone are shown in Fig. 7 for conditions initially and after 30 years of operation. Because the pre-treatment zone also provides for flow equalization, residence times within the PRB are more uniform when a pre-treatment zone is included. Longer and slightly more uniform residence times are also achieved with a pre-treatment zone after 30 years due to less fouling within the reactive zone.

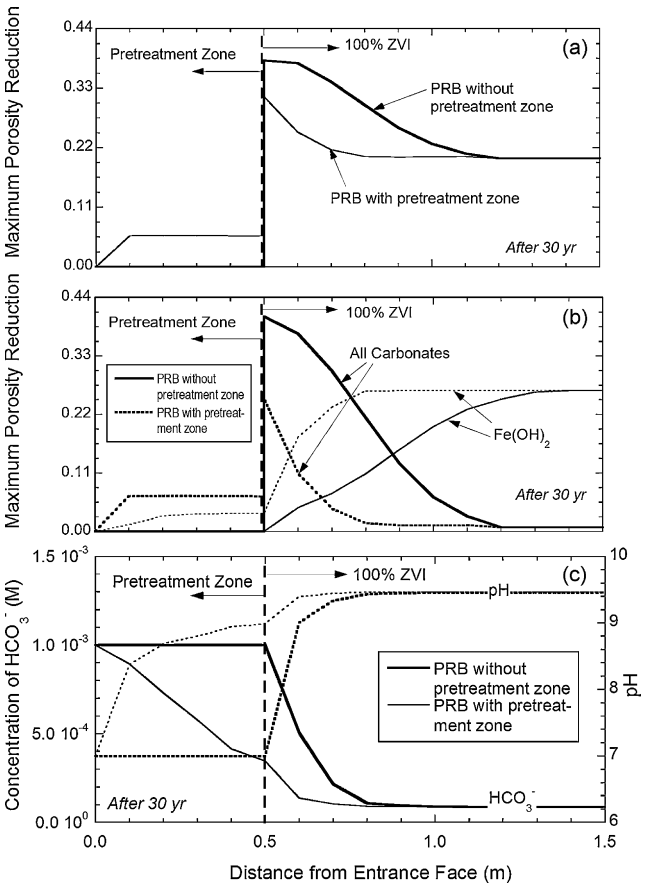

Fig. 6. Maximum porosity reduction (a), all carbonates and ferrous hydroxide precipitations (b), and concentration of bicarbonate and pH (c) after 30 years of operation as a function of distance from the entrance face of the PRB with and without gravel/ZVI pre-treatment zone.

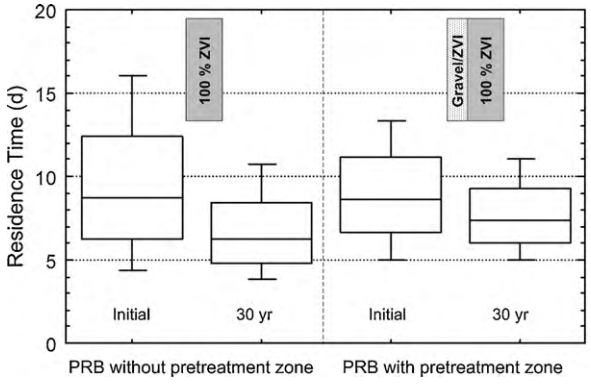

Fig. 7. Box plots of residence time in the PRB initially and after 30 years of operation with and without gravel/ZVI pre-treatment zone.

4.3. pH Adjustment

Simulations were conducted to evaluate the effectiveness of pH adjustment by fixing the OH^- concentration throughout the PRB at 10^{-5}, $10^{-5.5}$, 10^{-6}, or $10^{-6.5}$ M (i.e., pH = in 9.0, 8.5, 8.0 or 7.5). Average porosity reductions in the PRB without and with pH adjustment are shown in Fig. 8 as a function of distance from the entrance face of the PRB after 30 years.

pH adjustment results in a decrease in the average porosity reductions, with smaller porosity reductions obtained consistently as the pH is reduced. When the pH is dropped to 8.5, the peak average porosity reduction is eliminated, as $CaCO_3$ becomes

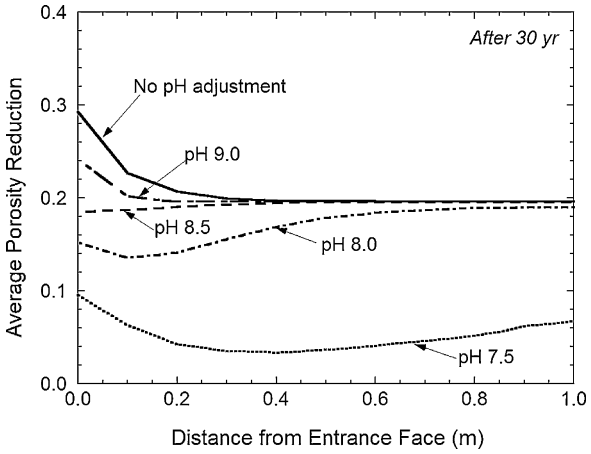

Fig. 8. Average porosity reduction after 30 years of operation as a function of distance from the entrance face of the PRB with and without pH adjustment.

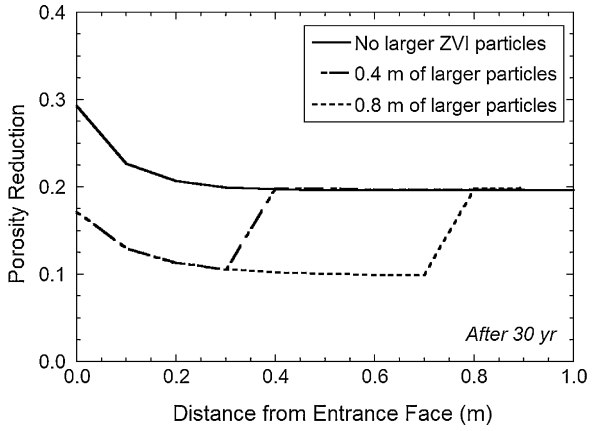

Fig. 10. Average porosity reduction after 30 years of operation as a function of distance from the entrance face of the PRB with various thicknesses of larger ZVI particles placed in front of the reactive zone and without larger ZVI particles.

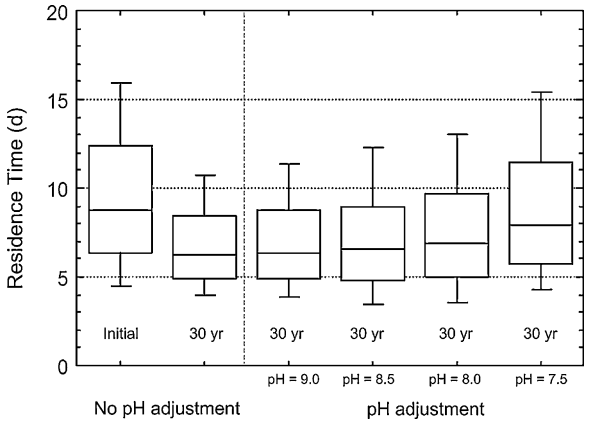

Fig. 9. Box plots of residence time in the PRB initially and after 30 years of operation with and without pH adjustment.

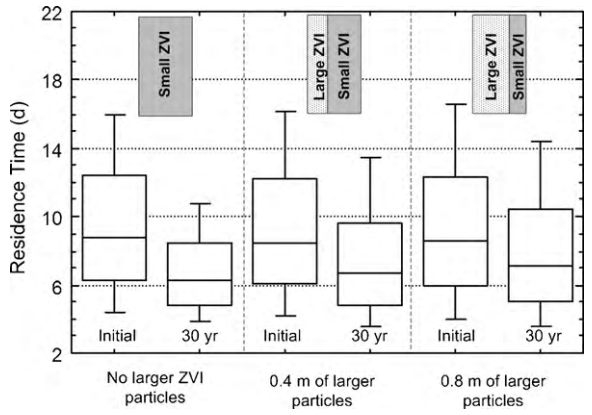

Fig. 11. Box plots of residence time in the PRB initially and after 30 years of operation with various thicknesses of larger ZVI particles placed in front of the reactive zone and without larger ZVI particles.

undersaturated and thus porosity reduction occurs only due to precipitation of $FeCO_3$ and $Fe(OH)_2$. The amount of $FeCO_3$ and $Fe(OH)_2$ formation is limited by the availability of ferrous ions in the solution which is controlled by the iron corrosion. When the pH is adjusted to 7.5, the peak of average porosity reduction returns, but is one third of the peak without pH adjustment.

Box plots showing the distribution of residence time in the PRB with and without pH adjustment at the onset of operation and after 30 years are shown in Fig. 9. pH adjustment to 7.5 decreases the reduction of residence time by fouling (the median residence time decreases 9% after 30 years at pH 7.5, compared to 28% without pH adjustment). Overall, however, the effect of pH control is modest.

pH controls the surface charge of the grains, which is also important factor of mineral settling on the surface of the grains and therefore the 'immobility' of the flocculated mineral is function of pH. This aspect is not considered in this paper and the model result is limited.

4.4. Large ZVI particles

Simulations were conducted to evaluate the effectiveness of increasing the size of ZVI particles by doubling the particle size at the entrance zone of the PRB. For simplicity, the porosity of the entrance zone was assumed to be the same as the porosity in the remainder of the reaction zone (i.e., packing of the ZVI is assumed to be controlled by angularity of the particles rather than their size). Iron surface area in the entrance zone was also assumed to be one-half the surface area in the remaining section. Hydraulic conductivity of the entrance zone with larger ZVI particles was assumed to be 400 m/d. The reduction in surface area in the entrance zone was assumed to have no effect on the ability of the PRB to provide sufficient treatment. However, in practice, the effect on treatment would need to be evaluated.

Average and maximum porosity reductions after 30 years are shown in Fig. 10 as a function of distance from the entrance face for PRBs with and without large ZVI particles. Larger ZVI particles result in a decrease in the average porosity reduction (0.12) in the entrance zone due to reduced corrosion associated with the larger particles. However, adding larger ZVI particles has no effect on the average porosity reduction in the remaining portion of the reactive zone containing original ZVI particles.

Box plots of residence time in the PRB with and without larger ZVI particles are shown in Fig. 11. Using larger ZVI particles in the entrance zone has little effect on the initial distribution of residence times. However, a higher median residence time is achieved after 30 years with larger particles in the entrance zone. After 30 years, the median residence time is 6% larger with a 0.4-m-thick entrance zone and 13% larger for 0.8-m-thick entrance zone with larger ZVI particles.

4.5. Mechanical treatment

Mechanical treatment was assumed to break down, dislodge, and uniformly redistribute the mineral precipitates, but

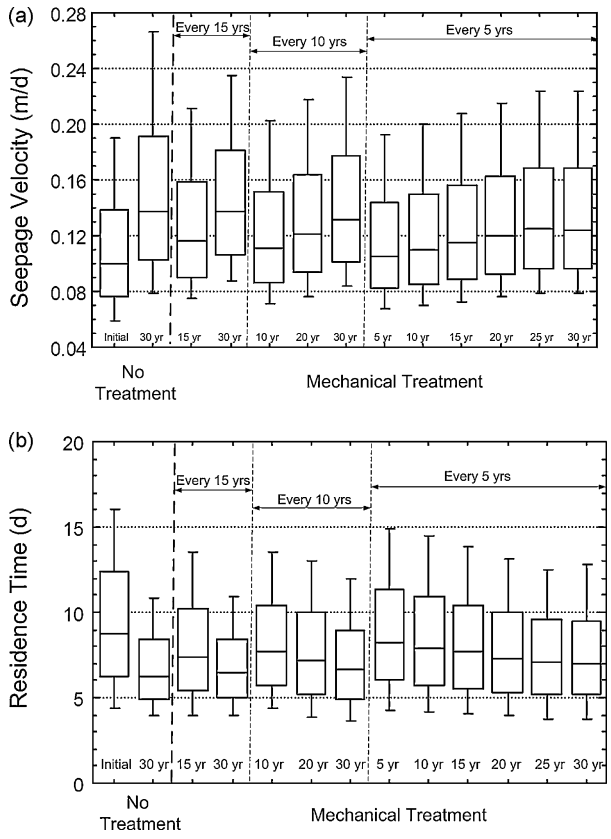

Fig. 12. Box plots of seepage velocity (a) and residence time (b) in the PRB from initially to after 30 years of operation with various mechanical treatment periods and without mechanical treatment.

not re-solubilize minerals. Mechanical treatment was simulated by redistributing the net accumulated mineral mass uniformly throughout the pore space in the PRB. Consequently, the PRB has uniform porosity initially and immediately after mixing. The iron surface area was assumed to be uniform immediately after the mechanical treatment.

Three scenarios were evaluated over 30 years of operation: (i) mechanical treatment after 15 years, (ii) treatment in each 10 years, and (iii) treatment in each 5 years. Box plots of seepage velocity in the PRB are shown in Fig. 12a for the PRB with and without mechanical treatment over 30 years. Mechanical treatment results in less variable and smaller seepage velocities at 30 years. For example, after 30 years, the median seepage velocity increases 10% in the PRB treated every 5 years and 15% in the PRB treated every 10 years, and 40% when the PRB is not treated. More frequent mechanical treatment can save more porosity reduction from fouling.

Box plots of residence time in the PRB with and without mechanical treatment over 30 years are shown in Fig. 12b. Larger residence times are maintained at 30 years with mechanical treatment, with the greatest impact obtained when the PRB is treated every 5 years.

5. Conclusions

Simulations were conducted with ground water flow model MODFLOW and reactive transport model RT3D to evaluate the effectiveness of five strategies intended to enhance the long-term hydraulic behavior of PRBs: (i) adding pea gravel equalization zones up gradient and down gradient of the reactive zone, (ii) placement of a sacrificial pre-treatment zone up gradient of the reactive zone, (iii) pH adjustment, (iv) using larger ZVI particles, and (v) mechanical mixing of the ZVI to break up and redistribute secondary minerals. For the five strategies, porosity reductions in the PRB over time were determined and the impact on residence times was investigated. Based on the simulation results, the following conclusions are drawn:

- Installation of pea gravel zones results in flow equalization and a more uniform distribution of residence times within the PRB, but has negligible impact on the median residence time in the near term and in the long-term (30 years). Average porosity reductions increase slightly when pea gravel zones are added, but maximum porosity reductions are reduced, particularly in deeper portions of the reactive zone.
- Sacrificial pre-treatment zones provide a region where the groundwater pH is elevated and mineral forming ions are consumed, resulting in less precipitation of secondary minerals within the reactive zone. Consequently, residence times within the PRB are less affected by mineral precipitation when a pre-treatment zone is employed. However, pre-treatment zones do not eliminate porosity reductions completely, as secondary minerals (e.g., $Fe(OH)_2$) still form within the reactive zone in response to iron corrosion.
- pH adjustment provides less OH^- for the mineral precipitation, resulting in smaller porosity reductions and decreases in residence time. The surface charge of the grains controlled by pH and corresponded mineral setting on the surface of the grains were not considered in this model study. Many of the contaminant degradation mechanisms are also influenced by pH. When the pH is lowered in the reactive media, the abiotic reductive dechlorination rate of TCE decreases and the driving force for metal hydroxide precipitation is also reduced.
- Using larger ZVI particles in the entrance of a PRB results in less mineral precipitation and fouling in the PRB, and increases the mean residence time. Use of larger particles with smaller surface may also affect treatment by the PRB. However, the effect on treatment was not evaluated in this study.
- Mechanical treatment has the potential to redistribute minerals within the pore space of the PRB, thereby resulting in a more uniform porosity reduction, a smaller peak porosity reduction, and longer residence times when conducted with sufficient frequency (every 5 years).
- None of the methods eliminated porosity reductions or prevented residence times from increasing during the 30-year service life of the PRB. Even if these treatment methods were employed, the effect of porosity reductions on residence time and treatment effectiveness would need to be evaluated.
- The comparisons among the five strategies are hard to be made quantitatively. The qualitative comparisons can be made among the five strategies. In terms of limiting impact of fouling on long-term hydraulic performance of PRB and easy installation/operation, the sacrificial pre-treatment zone method is the most favorable because it is effective to remove mineral forming ions and to result in less mineral precipitation. The pea gravel equalization zone is not effective to limit fouling. The pH adjustment and large ZVI particles method may alter the iron degradation rate of contaminant and offset the benefits of fouling reduction. The mechanical treatment requires frequent operation and maintenance which is not advantage for this in situ remediation technology.

Acknowledgments

Professor Prabhakar Clement of Auburn University provided the source code for RT3D along with valuable suggestions regarding its implementation. The authors are grateful for his assistance. The

authors are also grateful for the constructive review comments provided by two anonymous reviewers.

References

[1] EPA, Permeable Reactive Barrier Technologies for Contaminant Remediation, EPA-600-R-98-125, Washington, DC, 1998.
[2] D. Naftz, S. Morrison, J. Davis, C. Fuller, Handbook of Groundwater Remediation Using Permeable Reactive Barriers: Applications to Radionuclides, Trace metals, and Nutrients, Academic Press, California, 2002.
[3] P. Mackenzie, D. Horney, T. Sivavec, Mineral precipitation and porosity losses in granular iron columns, J. Hazard. Mater. 68 (1999) 1–17.
[4] D. Phillips, B. Gu, D. Watson, Y. Roh, L. Liang, S. Lee, Performance evaluation of a zerovalent iron reactive barrier: mineralogical characteristics, Environ. Sci. Technol. 34 (2000) 4169–4176.
[5] A. Henderson, A. Demond, Long-term performance of zero-valent iron permeable reactive barriers: a critical review, Environ. Eng. Sci. 24 (2007) 401–423.
[6] R. Wilkin, R. Puls, G. Sewell, Long-term performance of permeable reactive barriers using zero-valent iron: geochemical and microbiological effects, Ground Water 41 (2003) 493–503.
[7] R. Wilkin, S. Acree, R. Ross, D. Beak, T. Lee, Performance of a zerovalent iron reactive barrier for the treatment of arsenic in groundwater. Part 1. Hydrogeochemical studies, J. Contam. Hydrol. 106 (2009) 1–14.
[8] Y. Furukawa, J. Kim, J. Watkins, R. Wilkin, Formation of ferrihydrite and associated iron corrosion products in permeable reactive barriers of zero-valent iron, Environ. Sci. Technol. 36 (2002) 5469–5475.
[9] D. Phillips, D. Watson, Y. Roh, B. Gu, Mineralogical characteristics and transformations during long-term operation of a zerovalent iron reactive barrier, Environ. Qual. 32 (2003) 2033–2045.
[10] D. Sarr, Zero-valent iron permeable reactive barriers—how long will they last? Remediation 11 (2001) 1–18.
[11] R. Wilkin, C. Su, R. Ford, C. Paul, Chromium-removal processes during groundwater remediation by a zerovalent iron permeable reactive barrier, Environ. Sci. Technol. 39 (2005) 4599–4605.
[12] W. Kamolpornwijit, L. Liang, O. West, G. Moline, J. Sullivan, Preferential flow path development and its influence on long-term PRB performance: column study, J. Contam. Hydrol. 66 (2003) 161–178.
[13] P. Vikesland, J. Klausen, H. Zimmermann, L. Roberts, W. Ball, Longevity of granular iron in groundwater treatment processes: changes in solute transport properties over time, J. Contam. Hydrol. 64 (2003) 3–33.
[14] V. Zolla, F. Freyria, R. Sethi, A. Molfetta, Hydrogeochemical and biological processes affecting the long-term performance of an iron-based permeable reactive barrier, J. Environ. Qual. 38 (2009) 897–908.
[15] O. Jin, S. Jeen, R. Gillham, L. Gui, Effects of initial iron corrosion rate on long-term performance of iron permeable reactive barriers: column experiments and numerical simulation, J. Contam. Hydrol. 103 (2009) 145–156.
[16] L. Li, C. Benson, E. Lawson, Impact of mineral fouling on hydraulic behavior of permeable reactive barriers, Ground Water 43 (2005) 582–596.
[17] S. Morrison, Performance evaluation of a permeable reactive barrier using reaction products as tracers, Environ. Sci. Technol. 37 (2003) 2302–2309.
[18] A. Gavaskar, W. Yoon, J. Sminchak, B. Sass, N. Gupta, J. Hicks, V. Lal, Long Term Performance Assessment of a Permeable Reactive Barrier at Former Naval AITR Station Moffett Field. NAVFAC Report, CR 05-006-ENV, CA, 2005.
[19] J. Kenneke, S. McCutcheon, Use of pre-treatment zones and zero-valent iron for the remediation of chloroalkenes in an oxic aquifer, Environ. Sci. Technol. 37 (2003) 2829–2835.
[20] C. Geiger, C. Clausen, D. Reinhart, C. Clausen, N. Ruiz, J. Quinn, Using ultrasound for restoring iron activity in permeable reactive barriers, in: S.M. Henry, S.D. Warner (Eds.), Chlorinated Solvent and DNAPL Remediation: Innovative Strategies for Subsurface Cleanup, American Chemical Society: Distributed by Oxford University Press, Washington, DC, 2003, pp. 86–303.
[21] P. McMahon, K. Dennehy, M. Sandstrom, Hydraulic and geochemical performance of a permeable reactive barrier containing zero-valent iron, Ground Water 37 (1999) 396–404.
[22] D. Sorel, S. Warner, B. Longino, J. Honniball, L. Hamilton, Performance monitoring and dissolved hydrogen measurements at a permeable zero valent iron reactive barrier, in: S.M. Henry, S.D. Warner (Eds.), Chlorinated solvent and DNAPL remediation: Innovative Strategies for Subsurface Cleanup, ACS Symposium Series 837, American Chemical Society: Distributed by Oxford University Press, Washington, DC, 2003, pp. 278–285.
[23] C. Elder, C. Benson, G. Eykholt, Effects of heterogeneity on influent and effluent concentrations from horizontal permeable reactive barriers, Water Resour. Res. 38 (2002), Art. No 1152.
[24] S. Benner, D. Blowes, J. Molson, Modeling preferential flow in reactive barriers: implications for performance and design, Ground Water 39 (2001) 371–379.
[25] A. Gavaskar, N. Gumpta, B. Sass, Permeable Barriers for Groundwater Remediation: Design, Construction, and Monitoring, Battelle Press, Columbus, Ohio, 1998.
[26] D. Beak, R. Wilkin, Performance of a zerovalent iron reactive barrier for the treatment of arsenic in groundwater. Part 2. Geochemical modeling and solid phase studies, J. Contam. Hydrol. 106 (2009) 15–28.
[27] S. Jeen, K. Mayer, R. Gillham, D. Blowes, Reactive transport modeling of trichloroethene treatment with declining reactivity of iron, Environ. Sci. Technol. 41 (2007) 1432–1438.
[28] L. Li, C. Benson, E. Lawson, Modeling porosity reduction caused by mineral fouling in continuous-wall permeable reactive barriers, J. Contam. Hydrol. 83 (2006) 89–121.
[29] K. Mayer, D. Blowes, E. Frind, Reactive transport modeling of an in situ reactive barrier for the treatment of hexavalent chromium and trichloroethylene in groundwater, Water Resour. Res. 37 (2001) 3091–3103.
[30] R. Wilkin, P. Puls, Capstone Report on the Application, Monitoring, and Performance of Permeable Reactive Barriers for Ground-Water Remediation: Volume 1—Performance Evaluations at Two Sites. EPA 600-R-03-045a, U.S. Environmental Protection Agency, Cincinnati, Ohio, 2003.
[31] R. Vidic, Permeable Reactive Barriers: Case Study Review. Technology Evaluation Report: TE-01-01, Ground-Water Remediation Technologies Analysis Center, University of Pittsburgh, Pittsburgh, Pennsylvania, 2001.
[32] D. Blowes, R. Gillham, R. Puls, S. O'Hannesin, C. Hanton-Fong, J. Bain, An In-Situ Permeable Reactive Barrier for the Treatment of Hexavalent Chromium and Trichloroethylene in Groundwater-Performance Monitoring. EPA 600-R-99-095b, Washington, DC, 1999.
[33] M. Odziemkowski, T. Schmuacher, R. Gillham, E. Reardon, Mechanism of oxide film formation on iron in simulating groundwater solutions: Raman spectroscopic studies, Corros. Sci. 40 (1998) 371–389.
[34] Y. Roh, S. Lee, M. Elless, Characterization of corrosion products in the permeable reactive barriers, Environ. Geol. 40 (2000) 184–194.
[35] E. Reardon, Zerovalent, Irons: Styles of corrosion and inorganic control on hydrogen pressure buildup, Environ. Sci. Technol. 39 (2005) 7311–7317.
[36] J. Allison, D. Brown, K. Novo-Gradac, MINTEQA2/PRODEFA2, A Geochemical Assessment Model for Environmental Systems: Version 3.0 User's Manual. EPA-600/3-91-021, U.S. Environmental Protection Agency, Athens, Georgia, 1991.
[37] M. McDonald, A. Harbaugh, MODFLOW: A Modular Three-Dimensional Finite-Difference Ground-Water Flow Model, USGS Techniques of Water-Resources Investigations, Washington, DC, 1988.
[38] T. Clement, RT3D: A Modular Computer Code for Simulating Reactive Multi-Species Transport in 3-Dimensional Groundwater Aquifers. PNNL-SA-11720, Richland, Washington, 1993.
[39] B. Cochepin, O. Trotignon, C. Bildstein, V. Steefel, J. Lagneau, Van der lee, Approaches to modeling coupled flow and reaction in a 2D cementation experiment, Adv. Water Res. 31 (2008) 1540–1551.
[40] C. Zheng, G. Bennett, Applied Contaminant Transport Modeling, 2nd edition, Wiley-Interscience, New York, 2002.
[41] M. Anderson, Characterization of geological heterogeneity, in: G. Dagan, S. Neuman (Eds.), Subsurface Flow and Transport: A Stochastic Approach, Cambridge University Press, Cambridge, United Kingdom, 1997, pp. 23–43.
[42] M. Anderson, Movement of contaminants in groundwater: groundwater-transport-advection and dispersion, in: Groundwater Contamination, National Research Council, National Academy Press, Washington, DC, 1984, pp. 37–45.
[43] W. Stumm, J. Morgan, Aquatic Chemistry: Chemical Equilibria and Rates in Natural Waters, 3rd edition, John Wiley and Sons, New York, 1996.
[44] P. Lichtner, C. Steefel, E. Oelkers, Reactive Transport in Porous Media, Mineralogical Society of America, Washington, DC, 1996.
[45] A. Lasaga, Kinetic Theory in the Earth Sciences, Princeton University Press, New Jersey, 1998.
[46] K. Mayer, S. Benner, D. Blowes, Process-based reactive transport modeling of a permeable reactive barrier for the treatment of mine drainage, J. Contam. Hydrol. 85 (2006) 195–211.
[47] E. Bolton, A. Lasaga, D. Rye, Long-term flow/chemistry feedback in a porous medium with heterogeneous permeability: kinetic control of dissolution and precipitation, Abstr. Pap. Am. Chem. Soc. 105 (1999) 1–68.
[48] C. Ayora, C. Taberner, M. Saaltink, J. Carrera, The genesis of dedolomites: a discussion based on reactive transport modeling, J. Hydrol. 209 (1998) 346–365.
[49] K. Saripalli, P. Meyer, D. Bacon, Changes in hydrologic properties of aquifer media due to chemical reactions: a review, Crit. Rev. Environ. Sci. Technol. 31 (2001) 311–349.
[50] C. Zheng, Path3D: A Ground-Water Path and Travel-Time Simulator, S.S.Papadopulus & Associates, Inc., Maryland, 1991.
[51] S. Yabusaki, K. Cantrell, B. Sass, C. Steefel, Multicomponent reactive transport in an in situ zero-valent iron cell, Environ. Sci. Technol. 35 (2001) 1493–1503.
[52] K. Krauskopf, D. Bird, Introduction to Geochemistry, 3rd edition, McGraw-Hill, New York, 1995.
[53] E. Reardon, Anaerobic corrosion of granular iron: measurement and interpretation of hydrogen evolution rates, Environ. Sci. Technol. 29 (1995) 2936–2945.